Propagation of ion acoustic wave energy in the plume of a high-current LaB_6 hollow cathode

Benjamin A. Jorns*
Department of Aerospace Engineering, University of Michigan, Ann Arbor, Michigan 48109, USA

Christoper Dodson
Department of Mechanical and Aerospace Engineering, University of California, Los Angeles, California 90095, USA

Dan M. Goebel
Jet Propulsion Laboratory, California Institute of Technology, Pasadena, California 91109, USA

Richard Wirz
Department of Mechanical and Aerospace Engineering, University of California, Los Angeles, California 90095, USA
(Received 16 March 2017; published 23 August 2017)

A frequency-averaged quasilinear model is derived and experimentally validated for the evolution of ion acoustic turbulence (IAT) along the centerline of a 100-A class, LaB_6 hollow cathode. Probe-based diagnostics and a laser induced fluorescence system are employed to measure the properties of both the turbulence and the background plasma parameters as they vary spatially in the cathode plume. It is shown that for the three discharge currents investigated, 100 A, 130 A, and 160 A, the spatial growth of the total energy density of the IAT in the near field of the cathode plume is exponential and agrees quantitatively with the predicted growth rates from the quasilinear formulation. However, in the downstream region of the cathode plume, the growth of IAT energy saturates at a level that is commensurate with the Sagdeev limit. The experimental validation of the quasilinear model for IAT growth and its limitations are discussed in the context of numerical efforts to describe self-consistently the plasma processes in the hollow cathode plume.

DOI: 10.1103/PhysRevE.96.023208

I. INTRODUCTION

The onset and propagation of ion acoustic turbulence (IAT) has a critical role in many of the fundamental processes governing the plume of the hollow cathode discharge. For example, the growth of IAT in this electron source can lead to an enhanced electron resistivity [1]—one much higher than the classical resistivity from collisions—that can impact the local plasma density, temperature, species drifts, and plasma potential distribution [2]. Similarly, the wave energy in the IAT can contribute to nonclassical ion heating through both resonant and nonresonant processes, thereby leading to the potential formation of high energy ions [3–7]. Despite the apparent importance of the IAT to these physical processes in the cathode plasma, however, there are key aspects of this phenomenon that are not well-understood. The most fundamental of these is how the IAT actually propagates and grows in the plume. In addition to being of theoretical interest, there are practical reasons to understand this process. For instance, the hollow cathode is a critical electron source for many of the types of electric propulsion currently flown or proposed to fly in space. The need to reduce risk in the design and qualification of these systems for flight has driven the demand for increasingly high-fidelity predictive codes. But while the level of sophistication of models is improving, it has been recognized [8–10] that to fully self-consistently model these devices, it is necessary to account for the propagation of the IAT in the plume.

With this in mind, a number of studies have attempted to find a first-principles relation for the evolution of the IAT. The first of these employed simple closures—most notably a saturation model based on the so-called Sagdeev scaling [1]—to capture the effects of the turbulence [2,11]. However, while these efforts were able to match IAT-related plasma processes in the plumes of a select number of cathodes at relatively low discharge current (<25 A) [2,11], at higher currents and different geometries, these simplified models for the IAT evolution in the plume broke down [12]. In an effort to replace these simple closure models, more recent efforts have focused on finding first-principles relations for the IAT that self-consistently account for its propagation in an unsaturated state [8,9,13]. The evolution of the IAT predicted in these works, while showing promising initial results, has yet to be validated with direct experimental measurements. In light of these limitations of previous studies and the outstanding questions they invite about the correct hierarchy to describe the IAT, the need is thus apparent for a systematic, experimental study of its propagation in the cathode plume. The goal of this investigation is to address this need by focusing on the evolution of a key property of the IAT spectrum, the total energy density, which is believed to be the critical parameter for describing the turbulence's interactions with the background plasma properties. We seek to present from first principles an expression for the evolution of this energy density and then to validate our relation by comparing its predictions to direct experimental measurements.

The central hypothesis of this investigation is informed by our previous analytical work in Ref. [13] in which we posited that the total energy density of the IAT in the cathode plume could be modeled through a frequency-averaged, quasilinear formulation. Sary *et al.* recently explored a similar hypothesis in modeling a low-current discharge [9,10]. Our purpose here

*bjorns@umich.edu

is to revisit this quasilinear model and attempt to evaluate its validity against experimental measurements. With this in mind, we have organized this paper in the following way. Section II summarizes the derivation from quasilinear theory for the evolution of the total IAT energy density in the hollow cathode plume. This derivation is informed by assumptions consistent with known properties of the IAT in these devices. Section III provides an overview of the experimental configuration that we employed to examine the validity of our derived expression for the IAT propagation. This setup consisted of a 100-A class hollow cathode and a diagnostic suite for evaluating the local plasma parameters and wave properties. Section IV shows plots of the measured plasma parameters and properties of the IAT in the plume of the 100-A cathode. We use these direct measurements from the plasma to eliminate all free parameters in our quasilinear model except the energy density in the IAT. This allows us to predict, in a self-consistent way, the growth of this turbulent mode in the plume. These predictions for the IAT growth from the quasilinear model then are validated against direct experimental measurements. Section V includes a discussion of our experimental findings in the context of recent attempts to incorporate the evolution of the IAT in numerical models. We also outline the limitations as well as potential extensions of the quasilinear formulation.

II. QUASILINEAR FORMULATION FOR ENERGY DENSITY IN ION ACOUSTIC TURBULENCE

The ion acoustic instability is an electrostatic mode that can onset spontaneously in plasma regions like the hollow cathode plume where there is a strong electron drift. Ion acoustic turbulence (IAT) is, in a broad sense, the state that results when several of these acoustic modes with closely spaced frequencies and random phase are excited concurrently in the same region. In this section, we seek an expression for the evolution in the cathode plume of the total energy density of the modes in the IAT spectrum, $W_T = \int W_{\vec{k}} d\vec{k}$, where $W_{\vec{k}}$ denotes the energy density of the electrostatic mode with wave vector $\vec{k}$. We pursue this end first by considering a description of the evolution of the distribution function of modes in the plasma and then by performing an integral over k space of this relation to arrive at an expression for W_T. This approach, which we first described in Ref. [13], is in direct analog to the classical derivation of the plasma fluid equations that is performed by taking moments of the Boltzmann equations that govern each plasma species.

For propagating modes where the energy density is small, i.e., lower than the thermal energy in the plasma, a quasilinear form of the plasma wave kinetic equation (cf. Ref. [14]) is an appropriate hierarchy to describe the mode evolution:

$$\frac{\partial N_{\vec{k}}}{\partial t} + \vec{\nabla} \cdot (N_{\vec{k}} \vec{v}_g) - \vec{\nabla}_{\vec{k}} \cdot (N_{\vec{k}} \vec{\nabla} \omega_r) = N_{\vec{k}} [2\omega_i + \mathcal{C}(N_{\vec{k}})], \tag{1}$$

where we have defined the wave action, $N_{\vec{k}} = W_{\vec{k}}/\omega_r$, of the kth electrostatic mode, ω_r is the real component of the frequency of the kth mode, $\vec{v}_g = \vec{\nabla}_k \omega_r$ is the group velocity, ω_i denotes the growth rate, and $\mathcal{C}(N_{\vec{k}})$ captures nonlinear processes such as three wave interactions and nonlinear Landau damping. Just as the Boltzmann equation is a conservation relation for the particle distribution function, the wave action in Eq. (1) represents the local density distribution function of modes with wave vector $\vec{k}$, which is governed by spatial convection (first two terms), acceleration (third term), sources (fourth term), and collective effects due to interactions between modes (last term).

For the case of ion acoustic waves propagating in a plasma environment typical of the hollow cathode plume, we have explicit forms for the frequency, group velocity, and growth rate in Eq. (1) (cf. Refs. [14,15]):

$$\omega_r = c_s k + \vec{k} \cdot \vec{V}_i, \tag{2}$$

$$\vec{v}_g = \hat{k} c_s + \vec{V}_i, \tag{3}$$

$$\omega_i = \sqrt{\frac{\pi}{8}} (\omega_r - \vec{k} \cdot \vec{V}_i) \left(\frac{1 + 3\frac{T_i}{T_e}}{1 + 6\frac{T_i}{T_e}} \right) \times \left\{ \frac{\hat{k} \cdot \vec{V}_e}{v_{te}} - \left(3 + \frac{T_e}{T_i} \right)^{3/2} \exp\left[-\frac{1}{2} \left(3 + \frac{T_e}{T_i} \right) \right] \right\} - \frac{1}{2} \nu_i, \tag{4}$$

where $v_{te} = [k_b T_e / m_e]^{1/2}$ denotes the electron thermal velocity, $c_s = [k_b (T_e + 3T_i)/(m_i)]^{1/2}$ is the ion sound speed, k_b is the Boltzmann constant, $m_{e,i}$ denote the species mass, $T_{e,i}$ denotes the species temperature, $V_{e,i}$ denotes the drift velocities, and we have introduced a weak damping frequency, ν_i, due to ion-neutral collisions, the dominant momentum-changing collisions for ions in the plume. Equations (2)–(4) are valid subject to typical conditions of the hollow cathode plume [15]: $V_e \gg c_s, V_i$, $T_i/T_e \leqslant 1$, and $k\lambda_d \ll 1$, where λ_d is the Debye length. The physical interpretation of these relations in the context of Eq. (1) is that the electrostatic modes are acoustic in nature, propagating with the ion sound speed in the ion frame of reference. The source terms impacting their growth, encapsulated by ω_i, are a balance between inverse electron Landau damping [first term in Eq. (4)], ion Landau damping (second term), and ion-neutral collisions (third term).

We take the zeroth moment of Eq. (1) with respect to $\vec{k}$ to find a continuity equation for the evolution of the total density of acoustic modes:

$$\frac{\partial \int N_{\vec{k}} d\vec{k}}{\partial t} + \vec{\nabla} \cdot \left(\int N_{\vec{k}} \vec{v}_g d\vec{k} \right) = 2 \int \omega_i N_{\vec{k}} d\vec{k}, \tag{5}$$

where we have eliminated the third term on the left hand side of Eq. (1) by assuming a convergent spectrum of wave action at $k \to \infty$, and we have set the integral of the coupling term $\mathcal{C}(N_{\vec{k}})$ to zero under the assumption that the dominant nonlinear wave interaction for ion acoustic modes, nonlinear ion Landau damping, conserves the total number of wave quanta [1]. We can rewrite Eq. (5) in terms of our quantity of interest W_T if we make two additional, simplifying assumptions about the IAT in the cathode plume. First, we follow the treatment from the overview of IAT spectra presented in Ref. [16] in assuming that the density distributions of the direction of the wave vectors and their magnitudes are separable: $N_{\vec{k}} = N(k)N(\hat{k})$. Second, we make the approximation that the wave vectors

are confined locally to a small cone parallel to the electron drift direction, $\vec{k}||\vec{V}_e$, such that the density distribution in direction can be expressed $N(\hat{k}) \propto \delta(\hat{k} - \hat{V}_e)$. This assumption is consistent with the growth rate in Eq. (4) and the treatment in Ref. [1], which both show that the growth is dominant when the waves are collinear with the electron drift. Armed with these assumptions and the definition $W_{\vec{k}} = N_k \omega_r$, we use the expressions from Eqs. (2)–(4) to write Eq. (5) as

$$\frac{\partial W_T}{\partial t} + \vec{v}_g \cdot \vec{\nabla} W_T = \omega_0 W_T \left[\zeta_e - \zeta_i - \frac{\nu_i}{\omega_0} - \frac{\partial}{\partial t}\left(\frac{1}{\omega_0}\right) - \vec{\nabla} \cdot \left(\frac{\vec{v}_g}{\omega_0}\right) \right], \quad (6)$$

where we have defined

$$\zeta_e = \kappa \sqrt{2} M_e,$$
$$\zeta_i = \kappa \left(3 + \frac{T_e}{T_i}\right)^{3/2} \exp\left[-\frac{1}{2}\left(3 + \frac{T_e}{T_i}\right)\right],$$
$$\kappa = \sqrt{\frac{\pi}{2}} \left(\frac{1}{1 + \frac{\hat{V}_e \cdot \vec{V}_i}{c_s}}\right) \left(\frac{1 + 3\frac{T_i}{T_e}}{1 + 6\frac{T_i}{T_e}}\right). \quad (7)$$

Here we have introduced M_e, the electron Mach number, and the value $\omega_0 = \int \omega_r N_k d\vec{k} / \int N_k d\vec{k} = W_T / \int N_k d\vec{k}$. In keeping with the interpretation of wave action as a distribution function of the acoustic modes, this latter parameter denotes physically the average frequency of the IAT spectrum as it evolves in the cathode plume.

Equation (6) is a continuity equation for IAT energy density. The left-hand side captures the convection of the wave energy while the first three terms on the right-hand side denote contributions to the growth of the total energy in the IAT as it propagates: inverse electron Landau damping, ζ_e, ion Landau damping, ζ_i, and ion-collisional damping, ν_i/ω_0. The last two terms on the right-hand side represent changes in IAT energy density due to variations in the average frequency that are induced by gradients in the local plasma properties. This dependence is an expected result as the IAT energy density of an electrostatic mode is a function not only of the amplitude of the oscillation but also the frequency with which it propagates [14]. Decreases in average frequency along the propagation direction therefore should result in a reduction in the average energy density in the spectrum. This is reflected by the contributions shown in Eq. (6).

We can simplify the result in Eq. (6) by considering the characteristic length and time scales for the IAT evolution in the plume. Invoking the relations from Eqs. (2) and (3), we write $|\vec{v}_g/\omega_0| = \lambda_0$, where λ_0 is the average wavelength of the IAT spectrum, and $1/\omega_0 = \tau_0$, where τ_0 is the average period of oscillations of the modes in the spectrum. Denoting $\partial/\partial t \sim 1/\tau_c$ and $\vec{\nabla} \sim 1/L_c$ as the characteristic temporal and spatial evolution of the IAT spectrum as it evolves in the plasma, we make the assertion that

$$\left| \frac{\partial}{\partial t}\left[\frac{1}{\omega_0}\right] \right| \sim \frac{\tau_0}{\tau_c} \ll 1, \quad \left| \vec{\nabla} \cdot \left(\frac{\vec{v}_g}{\omega_0}\right) \right| \sim \frac{\lambda_0}{L_c} \ll 1. \quad (8)$$

This is a statement that the average wavelength and period of the propagating spectrum are smaller than the time and length scales over which these properties change. It is an assertion that is consistent with, and indeed a prerequisite of, the eikonal/WKB approximation that is the underlying assumption leading to the formulation of Eq. (1). We therefore neglect these terms in Eq. (6). Moreover, since our validation experiments in the following sections were conducted at steady-state, we are able to neglect the remaining time dependent terms. This leaves

$$\vec{v}_g \cdot \vec{\nabla} W_T = \omega_0 W_T \left[\zeta_e - \zeta_i - \frac{\nu_i}{\omega_0} \right]. \quad (9)$$

This end result is an expression, derived from first-principles and a quasilinear hierarchy, for the evolution of the total IAT energy density in the hollow cathode plume. It self-consistently accounts for variations in the background plasma parameters as well as in the average properties of the IAT itself (e.g., the group velocity and frequency). In the next section, we describe the experimental setup we employed to validate this governing relation by comparing its predictions to direct measurements of the IAT energy density in a high-current cathode plume.

III. EXPERIMENTAL SETUP

Figure 1(a) shows the experimental configuration for this investigation. The plasma source was a 100-A class, thermionically emitting hollow cathode, which as is described in more detail in Ref. [17], consisted of a 4.3-mm inner diameter LaB_6 emitting insert housed in a graphite tube. This graphite tube was capped with an orificed tungsten endplate and wrapped in a coaxial tantalum heater. The wrapped tube in turn was surrounded by a cylindrical 30-mm diameter graphite keeper with a 10-mm diameter orifice. During operation, the cathode discharged into a cylindrical, water-cooled anode placed ~30 mm downstream of the cathode keeper. The copper anode was concentric with the cathode centerline and lined with tungsten. The cathode setup was installed in the NASA Jet Propulsion Laboratory's (JPL) High-Bay test chamber, a 2.6 m × 5.2 m cryogenically pumped facility capable of base pressures of $\sim 10^{-7}$ T. We operated the hollow cathode at three discharge currents for this investigation, 100, 130, and 160 A, at a constant flow rate of 15 sccm (defined at STP conditions of 760 T and 25 °C) of research-grade xenon. The background pressure remained ~1–1.2 × 10^{-5} T xenon for all three test conditions.

We employed a combination of translating probes and optical diagnostics to characterize the cathode plume properties. For measurements of the IAT, we implemented a translating set of two ion saturation probes with tungsten electrodes spaced apart axially by 5 ± 1 mm (cf. Ref. [15]) and adopted the Beall technique [18] to examine the cross-correlation between the probes' time-dependent signals. In this way, we were able to determine the spatial evolution of the dispersion relation of the IAT. Similarly, we measured the potential amplitudes of the modes in the IAT by relating the ion saturation fluctuations on a single probe in the array, $\tilde{i}_{sat}$, to potential fluctuations with the electrostatic approximation $\phi \approx (T_e/q)(\tilde{i}_{sat}/\bar{i}_{sat})$, where $\bar{i}_{sat}$ denotes the time-averaged value and q is fundamental charge. For the background plasma parameters, we implemented a

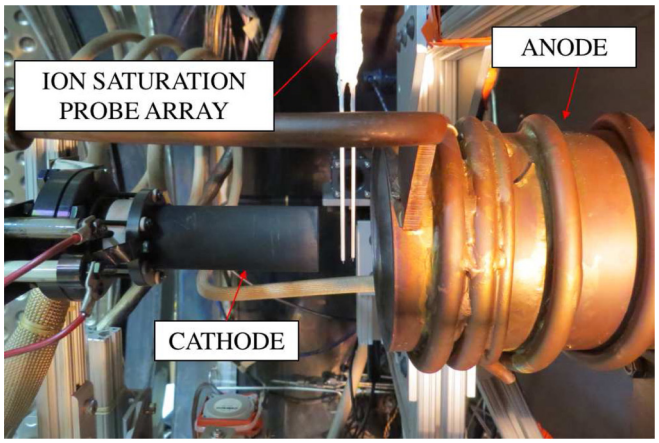

(a)

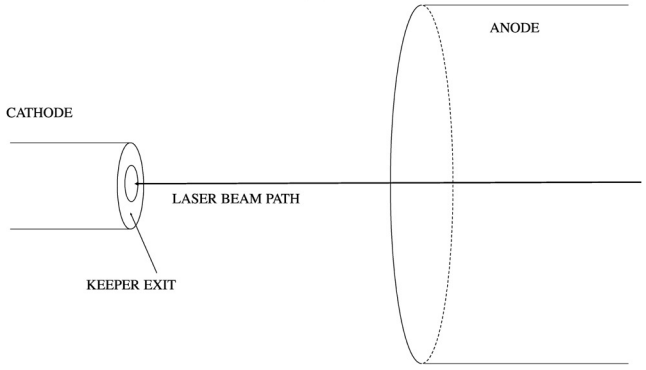

(b)

FIG. 1. (a) Experimental setup of the 100-A LaB_6 hollow cathode and cylindrical anode. The ion saturation probe array for dispersion measurements is also shown. (b) Schematic of the experimental setup illustrating the beam path for the laser induced fluorescence system. All experimental measurements are referenced axially with respect to the surface denoted "keeper exit" and radially with respect to the cathode centerline.

translating, swept Langmuir probe with a 2-mm-long and 0.5-mm-diameter tungsten tip, and we applied a semilog analysis and thin-sheath approximation to characterize the electron temperature and plasma density, respectively [19].

We inferred the ion drift velocity and ion temperature from measurements of the ion velocity distribution function (IVDF) made with a translating laser induced fluorescence (LIF) system. This diagnostic, which is described in more detail for our cathode setup in Ref. [7], employed a nonresonant scheme to interrogate the $5d^2F_{7/2} \rightarrow 6d_2^{5/2}$ metastable state of xenon ions. During operation, the LIF system injected a collimated laser beam into the region of interest and measured the fluoresced light from a portion of the plasma intersected by the beam. This yielded a measurement of the component of the IVDF along the direction of beam injection. For this investigation, we aligned the beam direction to the cathode centerline [Fig. 1(b)] by injecting the laser beam through the anode and along the setup's central axis. As we will discuss in the following sections, although this scheme only allowed us to measure the axial projection of the IVDF along cathode centerline, it yielded sufficient information to evaluate the validity of the IAT growth we derived in Sec. II.

The region of interrogation for our measurements extended from 0–19 mm downstream of the cathode keeper exit for the LIF measurements and 3–19 mm for the probe measurements. The spatial resolution was 2 mm and 4 mm for the probe and LIF measurements, respectively. The velocity resolution of the LIF measurements was ∼100 m/s.

We briefly note here that while LIF is an inherently noninvasive diagnostic, the use of physical probes raises potential concerns about these diagnostics perturbing the local plasma properties that they are intended to measure. This is a known effect in some low-temperature systems (cf. Refs. [20,21]). In our setup, the support structures for our probes were ∼1 mm in diameter and were oriented parallel to the keeper surface along the radial direction. At the keeper, the probe cross-sectional area presented to the plasma flow therefore was ∼6% of the total plasma cross-sectional area. Although Langmuir probes of comparable dimensions have been employed in similar hollow cathode plasma experiments with measurements seemingly corroborated by semi-empirical numerical models (cf. Refs. [22,23]), we were not able to quantify independently here the potential impact of these probes on the local plasma properties. We did observe, however, some evidence suggesting that the probes in our setup may have influenced the cathode operation. Although the visible structure of the plasma did not appear to change when the probes were inserted, the discharge voltage from the anode to the cathode decreased by 5–10% when the probes were placed closest to the cathode exit plane. We therefore cannot discount the possibility that the probes introduced perturbative effects in the plasma, and we thus report in this investigation plasma properties with this understanding.

IV. RESULTS

We present in this section experimental measurements for the purpose of validating our model from Sec. II. We first use data on the plasma and IAT properties to determine numerical values for the coefficients in Eq. (9) and solve for the predicted evolution of the IAT energy density. These predictions then are compared to direct experimental measurements. Since Eq. (9) is multidimensional, this approach in principle would require an assessment of the two-dimensional spatial distribution of the plasma and IAT properties in a cross-section of the axisymmetric cathode plume. However, we demonstrate here that, in light of the properties of the plume's shape, we can reduce Eq. (9) to a quasi-one-dimensional formulation. To this end, we show in Fig. 2 two-dimensional plots of the plasma density and electron temperature at the 160 A operating condition. We generated these figures by mapping data in the upper half of the domain and assuming symmetry across the cathode centerline. As can be seen from Fig. 2(a), the core of the cathode plume had a radius dictated by the keeper diameter, 10 mm, and this core remained collimated in the near field region downstream of the keeper. Similarly, as Fig. 2(b) shows, the electron temperature in this core region was nearly isothermal with a slight increase downstream of the keeper. Since these features—a near isothermal temperature and collimated plume—were exhibited for all three operating conditions we examined, we can simplify our analysis from Sec. II by making the quasi-one-dimensional approximation

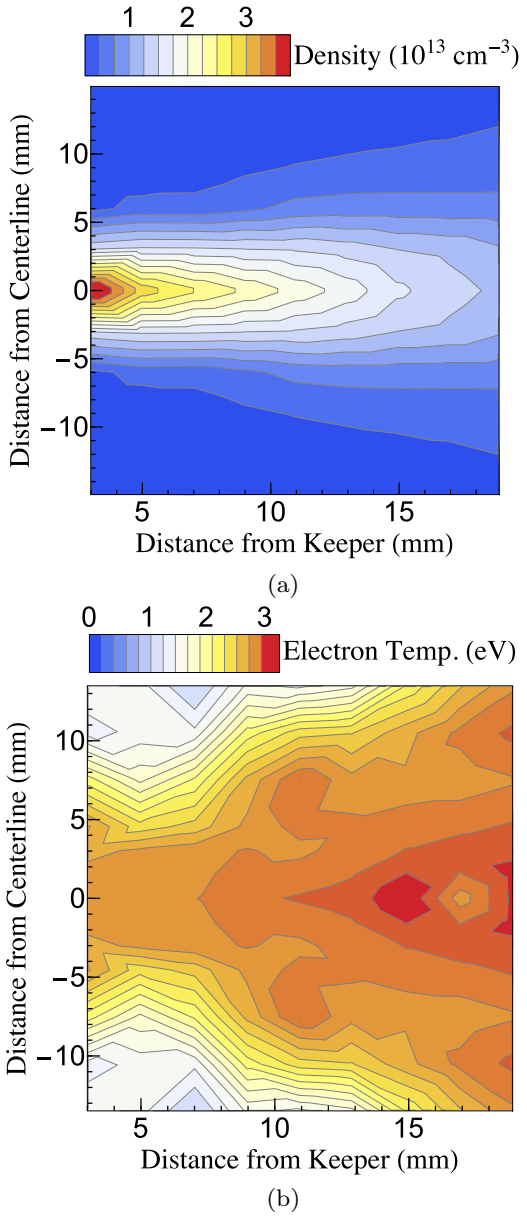

FIG. 2. Two-dimensional maps of (a) plasma density and (b) electron temperature in the hollow cathode plume for a discharge current of 160 A and flow rate of 15 sccm. The diameter of the keeper orifice at the exit plane (located at 0 mm) is 10 mm.

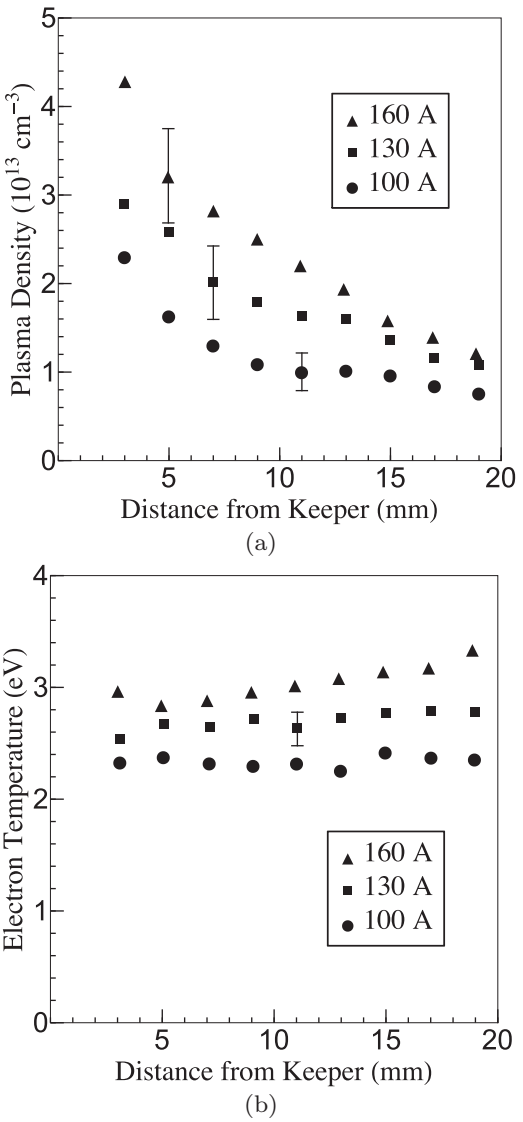

FIG. 3. (a) Plasma density and (b) electron temperature along centerline for the three investigated discharge currents.

that near the cathode centerline the IAT energy density is uniform in the transverse direction. We similarly make the assumption that the electron drift along the cathode centerline is collinear with this direction. These simplifications allow us to reduce Eq. (9) to one dimension:

$$v_{g(x)}\frac{\partial W_T}{\partial x} = \omega_0 W_T\left[\zeta_e - \zeta_i - \frac{\nu_i}{\omega_0}\right]_{\hat{V}_e=\hat{x}}, \qquad (10)$$

where $\hat{x}$ is parallel to the setup's central axis and we have evaluated the growth terms with the substitution $\hat{V}_e = \hat{x}$. Subject to these simplifications and in consideration of the explicit forms for the growth terms [Eq. (7)], we therefore now only need to examine the spatial dependence of the remaining plasma parameters along cathode centerline.

With this in mind, we present in Sec. IV A values for the plasma and neutral densities, ion and electron temperatures, ion and electron drift velocities, and the IAT's group velocity and average frequency. We then compare in Sec. IV B direct measurements of the IAT energy density in the cathode plume to the predictions found by solving Eq. (10), where the coefficients for the energy density terms have been evaluated with the background parameters from Sec. IV A.

A. Background plasma and IAT measurements on cathode centerline

1. *Plasma density and electron temperature*

We show in Fig. 3 the axial dependence of the plasma density and electron temperature for the three experimental conditions we examined. The error in the density measurements reflects the uncertainty in the probe dimensions as well as in our estimates for the ion saturation current. This latter variability stemmed from this parameter's weak dependence

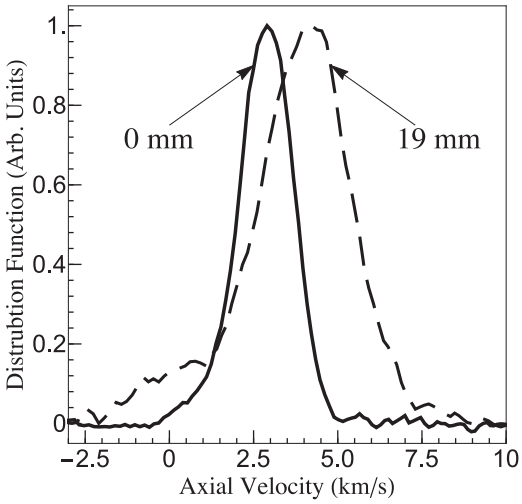

FIG. 4. Representative plots of the axial ion velocity distribution function at two positions along the cathode centerline. The operating condition was 130 A with 15 sccm flow.

on probe bias. The electron temperature error was estimated by bootstrapping via case-resampling the data from the linear part of the semilog plot yielded by each probe sweep. As the results in Fig. 3 show and as is consistent with Fig. 2, the electron temperature was nearly constant with position. The density, on the other hand, decreased along the centerline with a near power law dependence.

2. *Ion velocity and temperature*

We show in Fig. 4 two plots of the axial component of the IVDF along the cathode centerline taken at the operating condition of 130 A and 15 sccm. These cases illustrate three salient features we observed in the transition from the upstream region (0–15 mm from the keeper exit) to the downstream region of the plume. First, although the IVDFs remained approximately Gaussian with position, the drift velocity (denoted approximately by the peak in the IVDF), increased downstream. This indicates the ions underwent a bulk acceleration. Second, the width of the IVDF broadened with downstream position. This suggest the ions were heated leading to an increase in effective ion temperature. Finally, we found that in all three operating conditions, a second peak began to emerge in the downstream IVDF that was centered at 0 km/s. This second population could be attributed to charge-exchange collisions between the neutrals and ions, and previous studies [7] have shown that it can be dominant in the anode region. For our investigation, however, where we confined our study to the domain only extending 19 mm downstream of the keeper, the amplitude of this secondary population remained small—lower than 20% of the bulk peak.

We limited our assessment of the bulk ion plasma parameters to a consideration of the properties of the larger amplitude population. By applying a drifting Maxwellian fit to this dominant, higher velocity peak in the IVDF and using the best fit parameters, we estimated both the drift velocity and temperature. The results as a function of axial position are shown in Fig. 5, where the error bars stem from two sources: uncertainty in the fit parameters and a 5–20% systematic error

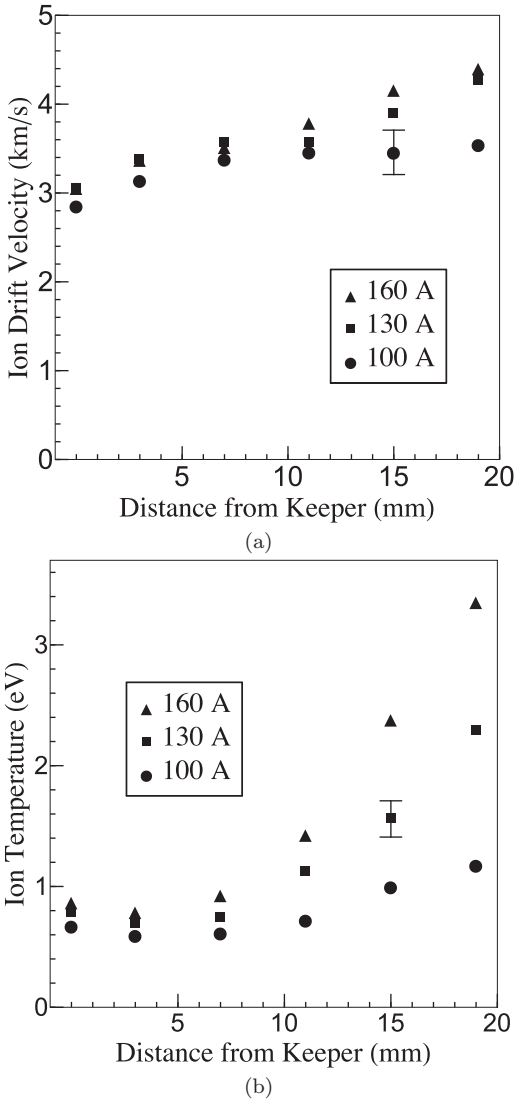

FIG. 5. (a) Ion drift velocity along cathode centerline and (b) ion temperature along cathode centerline.

introduced by the slight power saturation of the LIF transition by the laser beam power. We note two trends from these results that are consistent with our observations from the raw IVDFs in Fig. 4. First, as Fig. 5(a) shows, the ions experienced a gradual downstream acceleration in all three operating cases. The mechanism responsible for this slight acceleration is not explored here, but possible drivers include gradual potential or pressure gradients in the cathode plume. Second, as exhibited by Fig. 5(b), the ion temperature increased in all three cases from a common baseline of ∼0.8 eV. The degree of the heating scaled with the discharge current, and for the higher-current, 130 A and 160 A operating conditions, it almost reached parity with the electron temperature at the edge of the domain [Fig. 3(b)]. This rapid increase in ion temperature cannot be explained by classical mechanisms [8], and indeed, previous work [7,15] has shown that it is correlated with the IAT energy density. The physical interpretation from these previous treatments is that the temperature increase may be attributed to non-resonant heating due to ion sloshing as well as resonant effects through ion Landau damping of the IAT.

We briefly note here that the presence of these types of high-energy ions in the hollow cathode plume is a subject of practical interest for this technology's development. Indeed, nonclassical energetic ions are believed to play a governing role in contributing to the anomalously high erosion of the keeper's downstream surface that has been observed during wear tests of these devices (cf. Refs. [11,24]). While a number of mechanisms previously have been proposed to explain the formation of these high energy ions at the keeper, we have conjectured (Ref. [6]) that the type of IAT-driven heating that we observe in this work [Fig. 5(b)] may be the dominant contributor. We cannot, however, use our current results to support this conjecture as we have confined our observations to the centerline where the IVDFs show unambiguously that the heated ion population drifts away from the cathode keeper. This does not necessarily rule out the IAT as a dominant driver for the ion heating at the keeper. It is possible, for example, that off the central axis of the cathode and closer to the keeper radius, the IAT propagation may be oblique with respect to the centerline. Since the IAT heating occurs in the direction of wave propagation, these oblique components could in principle contribute to the production of energetic ions with some component of velocity directed back toward the keeper. This hypothesis is examined in more detail in Refs. [6,7]. For the purposes of this investigation, however, where our goal is to explore the governing equation of the IAT energy density, we simply treat the ion temperature as an input parameter for determining the validity of Eq. (10).

3. Electron Mach number

While we are able to measure several of the key plasma properties necessary to evaluate the coefficients in Eq. (10) explicitly, we did not have the diagnostic capability to measure directly the electron drift velocity. We can, however, use the plasma parameters available to us provide estimates for this value. To this end, we assume a constant cross-section of the core plasma (as is consistent with the plot in Fig. 2) and approximate the flow as longitudinal in this cross-section. The average electron drift velocity along the centerline thus is given by $V_e \approx I_D / \int_0^{r_e} 2\pi q n_0(r) r dr$, where $r_e \sim 5$ mm is the edge of the beam dictated by the orifice radius and I_D is the discharge current. Following this prescription and employing the data from Fig. 3, we show in Fig. 6 the estimated average electron Mach numbers on centerline. The representative error bars reflect the propagation of uncertainty from the error in the plasma parameter measurements. The average values, on the order of one, are suggestive of the strong electron drift in these devices, which serves as the energy source for driving the IAT unstable. The gradual acceleration of the electron velocity downstream can be attributed to the decrease in density in the cathode plume.

4. Ion-neutral collision frequency

The ion-neutral collision frequency is determined with the prescription $\nu_i = \sigma V_i n_n$, where V_i denotes the local ion velocity and σ is the charge-exchange cross section of 10^{-18} m^2 [25]. Since we did not have a direct measurement of the neutral density in the cathode plume, we make an upperbound estimate by equating the cathode flow rate to the thermal flux of neutrals through the keeper orifice. This gives an exaggerated value for the density along centerline since it neglects the loss of neutrals to ionization as well as the decrease due to expansion. However, as we will discuss in Sec. IV B, this is an acceptable approximation. We estimate the thermal speed of the neutrals exiting the keeper by using the ion temperature at this point (an assumption of thermal equilibrium consistent with previous validated models of the highly collisional regime inside the cathode tube [26]) to find for a flow rate of 15 sccm an upper bound estimate for the neutral density of $n_n \sim 7 \times 10^{13}$ cm^{-3}. At the exit plane of the keeper, this yields an approximate ion neutral collision frequency [employing the results from Fig. 5(a)] of $\nu_{in} \approx 200$ kHz.

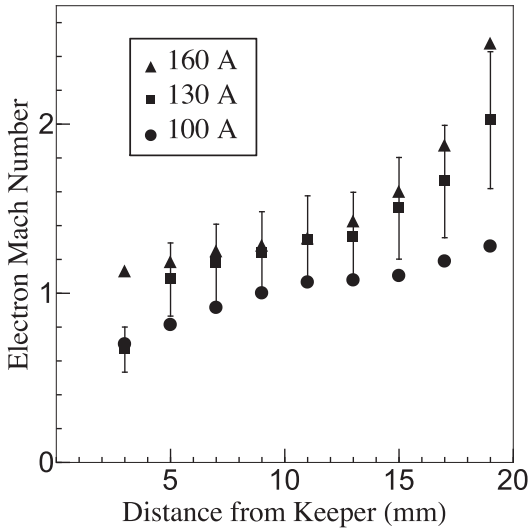

FIG. 6. Estimated values for the electron Mach number along cathode centerline.

5. Average IAT frequency

In addition to a number of background plasma parameters, our results from Sec. II show that to evaluate the coefficients in Eq. (10), we also require estimates of two average properties of the IAT: the spatial evolution of the average frequency, ω_0, and the component of the group velocity, $v_{g(x)}$ along centerline. As outlined in Sec. II, we can determine the average frequency with the prescription $\omega_0 = \int W_{\vec{k}}(\omega_r) d\omega_r / \int (W_{\vec{k}}(\omega_r)/\omega_r) d\omega_r$, where we have made the transformation of the integral over wave number to frequency space with the relation Eq. (2). Evaluating this expression requires an experimental measurement of the IAT spectrum as a function of frequency, which we can estimate for ion acoustic waves using the canonical definition for planar electrostatic modes (cf. Refs. [14,15]):

$$W_{\vec{k}}(\omega_r) = n_0 \frac{q^2 \phi_{\omega_r}^2}{T_e(1 + 3T_i/T_e)} \left[1 + \frac{V_i}{c_s}\right], \qquad (11)$$

where n_0 is the plasma density, ϕ_{ω_r} is the potential amplitude of the kth mode with frequency ω_r, and V_i denotes the axial component of the ion velocity. We use our results from the previous section to evaluate the temperature, density, and drift velocity in Eq. (11). And per the description in Sec. III, we use

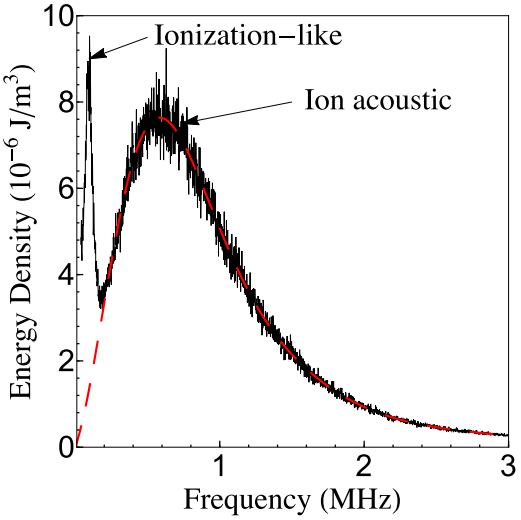

FIG. 7. Power spectrum of IAT energy density at a position 11 mm downstream of the keeper for the operating condition of 130 A and 15 sccm. The result exhibits two dominant oscillations in the plasma: ionization-related and ion acoustic. The dashed line is a 25-degree best-fit polynomial to the IAT spectrum.

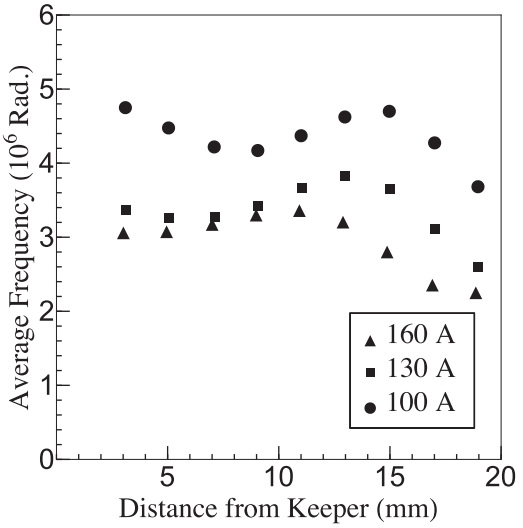

FIG. 8. The average angular frequency of the IAT spectrum, ω_0, along cathode centerline for the three operating conditions investigated.

relative fluctuations in ion saturation to estimate the plasma potential amplitude.

Figure 7 shows a representative plot of the power spectrum of the energy density of the IAT at a position 11 mm downstream of the keeper for the operating condition of 130 A and 15 sccm. The spectrum exhibits two distinct peaks: one at high frequency, 600 kHz, and one at a lower frequency, 90 kHz. The nature of these two peaks have been discussed in our previous work [15], where we identified the low frequency oscillation with the coherent, ionization-like mode first examined in detail by Goebel *et al.* [27] and the other more diffuse spectrum with the acoustic turbulence. For the purposes of this investigation, we isolated the contribution of the IAT to the spectrum by employing a 25-degree polynomial fit to the higher frequency peak (shown as a dashed line in Fig. 7).

We applied this fit to each measured IAT spectrum and subsequently used the resulting functions to evaluate the average frequency. Figure 8 shows the result expressed in radians as a function of axial position, where we can see ω_0 remained approximately constant in the region immediately downstream of the keeper (0–12 mm) and subsequently decreased with distance. The reason for this characteristic spatial dependence, which is qualitatively similar in all three cases, is not evident from our formulation in Sec. II. Uncovering the underlying causes of this trend is beyond the scope of this investigation, though we do reserve a brief discussion for possible models for this average frequency for Sec. V.

6. IAT group velocity

We determined the other critical property of the IAT, the group velocity, in two different ways. First, we followed the technique outlined in Ref. [15] (Figs. 3 and 4) to infer directly the group velocity of the spectrum from experimental measurements of the dispersion relation. This procedure involves fitting a line to the Beall plot generated from an analysis of the fluctuations on the ion saturation probe array. The results from this technique are shown in Fig. 9, where we note that due to the presence of other, low-frequency modes in the plume (see Fig. 7), we were only able to resolve the dispersion of the IAT clearly with this technique for positions greater than 5 mm from the keeper. As a check on these direct measurements for group velocity, we evaluated the analytical result, Eq. (3), with the data shown in Figs. 3(b) and 5. There is marked agreement between the calculated and measured values, which is a direct validation of the wave dispersion we presented in Sec. II. This close correspondence between theory and measurement also provides insight into what drives the trends in group velocity shown in Fig. 9. In

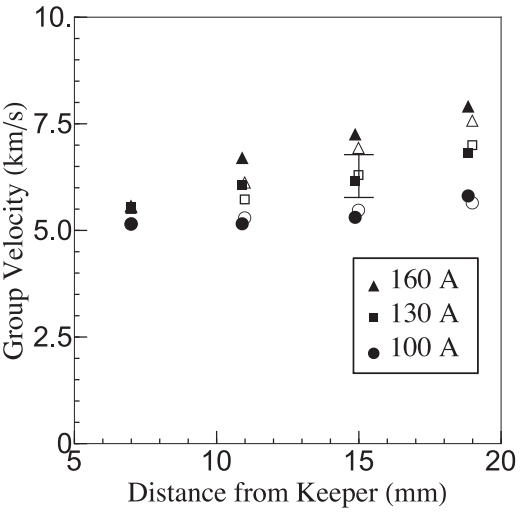

FIG. 9. Group velocity along axial centerline that was measured from best fits to dispersion plots (solid) and calculated from plasma parameters per Eq. (3) (open). The measured group velocity was estimated by assuming a probe separation of 4 mm.

particular, per Eq. (3), the group velocity in the laboratory frame increases both with the ion sound speed, which depends on ion temperature, as well as the ion drift velocity. The rise in both of these plasma parameters downstream of the cathode exit therefore can explain the same observed trends in group velocity. As a caveat to this finding, we note here that the good agreement between the measurement and prediction is predicated on assuming a probe spacing in the array of 4 mm—the lower bound on the uncertainty in probe separation (nominally spaced at 5 ± 1 mm). We chose this value as it yielded the best quantitative agreement with the calculated group velocities. A different choice of probe separation would lead to a higher estimate of group velocity but still capture the same trends as exhibited by the calculated data.

B. Growth rates

1. Predicted growth

With the results from the previous section, we now can evaluate the predicted growth of the IAT energy density along the cathode centerline from our quasilinear formulation in Sec. II. The method we follow here is to use the plasma and IAT properties from the previous section to calculate the coefficients and growth factors in Eq. 10. This only leaves the total energy density, W_T, as the free parameter that we must solve for in the governing equation. The advantage of this technique is that by using direct measurements of the plasma to determine the IAT evolution at steady state, any predicted growth will be self-consistent with the plasma processes in the plume. With this in mind, we show in Fig. 10(a) the calculated growth factors, ζ_e, ζ_i, and ν_i/ω_0 along the channel centerline for the representative operating condition of 130 A and 15 sccm. The effect of ion-neutral collisions is negligible compared to the other growth factors despite our overestimate of its size in Sec. IV A. This observation is borne out in the other operating conditions as well. By contrast, the ion Landau damping term is nonnegligible, which can be attributed to the finite ion temperature in the plume. The waves overall are not damped, however, because the growth driven by inverse electron Landau is still larger, $\zeta_e > \zeta_i$. We therefore anticipate, in light of Eq. (10), that the IAT energy density should grow in the plume.

We quantify this predicted growth explicitly from Eq. (10) by defining a local, one-dimensional spatial growth rate along centerline:

$$k_{i(L)} = \frac{1}{W_T}\frac{\partial W_T}{\partial x} = \frac{\omega_0}{v_{g(x)}}\left[\zeta_e - \zeta_i - \frac{\nu_i}{\omega_0}\right]. \qquad (12)$$

We in turn evaluate this parameter at each axial location by substituting the measured ω_0 and $v_{g(x)}$ as well as the measured growth factors. The resulting values for $k_{i(L)}$ are shown in Fig. 10(b) where the errors reflect the propagation of the uncertainty from the experimental data. It is evident from this plot that in all three cases, the predicted spatial growth is approximately constant within error bars. This constancy is a direct result of the convolution of the various contributions to $k_{i(L)}$: although the dominant growth factor from the electron Landau damping term, ζ_e, increases with position [Fig. 10(a)], the average frequency, ω_0, decreases (Fig. 8). Taken in the context of Eq. (10), these predictions of the growth from

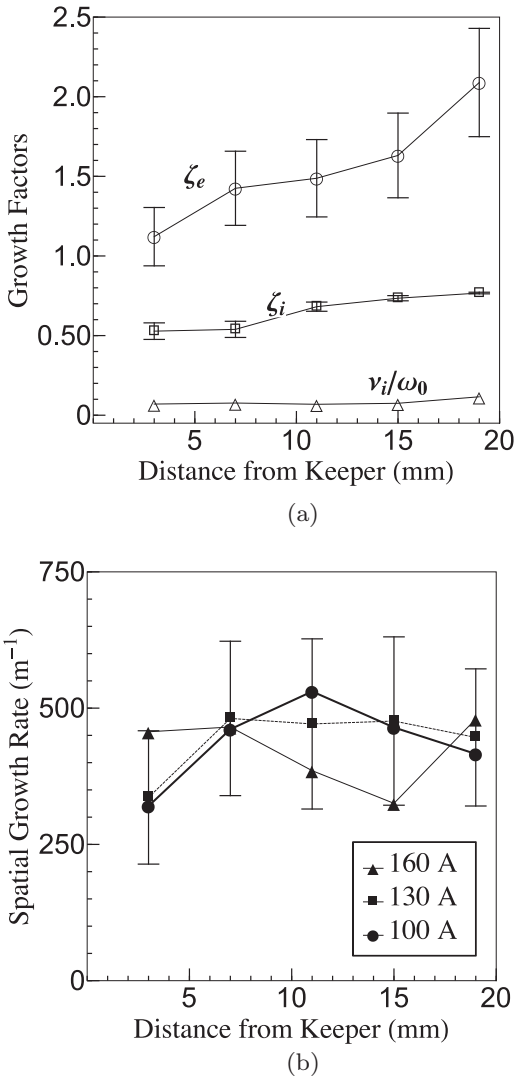

FIG. 10. (a) The magnitude of calculated non-dimensional growth factors for the IAT for the operating condition of 130 A and 15 sccm. $\zeta_{e,i}$ stems from electron and ion Landau damping, and ν_i is the ion-neutral collision frequency. (b) Calculated spatial growths for the IAT for the three operating conditions investigated.

Fig. 10(b) suggest that (1) the total growth in the IAT energy density should be exponential and (2) that the growth rate should be approximately the same for all three operating conditions.

2. Measured growth

We examine here the validity of the quasilinear formulation by comparing its predictions [Fig. 10(b)] to direct experimental measurements for the growth of the energy density, W_T. We calculated this latter quantity by integrating over the best-fit functions to the measured IAT spectrum introduced in Sec. IV A 5. The measured result, shown in Fig. 11, demonstrates that although the magnitude of the energy density depended on the discharge current, its evolution in the region immediately downstream of the keeper exhibited similar exponential growth in all three cases. This is directly in line with the two predictions from the quasilinear formulation from Eq. (12) and shown in Fig. 10. At the two higher current cases,

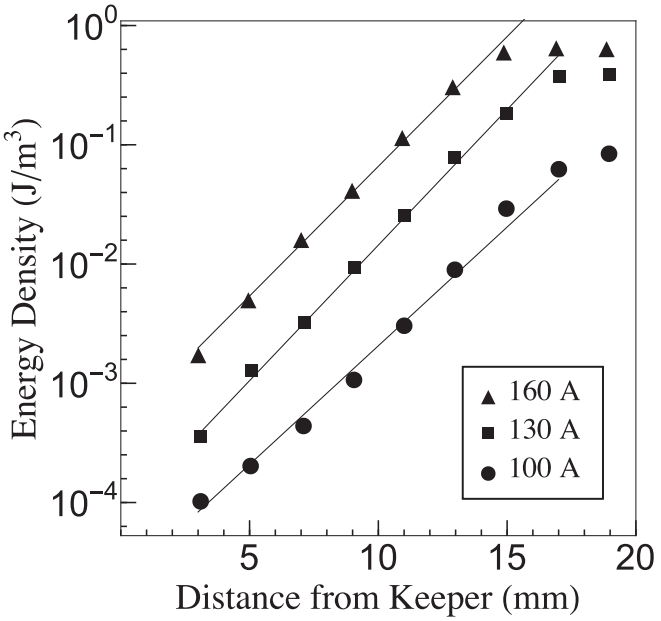

FIG. 11. Semilog plot of the total IAT energy density along cathode centerline for the three investigated operating conditions.

this exponential growth did appear to give way to a plateau at the downstream edge of the domain, but this may represent a type of saturation at large amplitudes where the quasilinear formulation does not apply. We reserve a discussion of this latter trend for the following section.

In the upstream region where the exponential growth was dominant, however, we can compare the measured growth to the predicted values from quasilinear theory. In particular, we fit lines to the semilog plots where they are linear and compare the resulting average spatial growths, k_i, to the mean values of the calculated spatial growths, $\langle k_{i(L)} \rangle$ from Fig. 10(b). The comparison is shown in Fig. 12, where the uncertainty bars reflect the errors in the estimates for the calculated spatial growths from Fig. 10(b). From this result, we can see that within experimental error, there is marked agreement between the quasilinear prediction and the actual measured growth of the IAT energy density. This close correspondence between

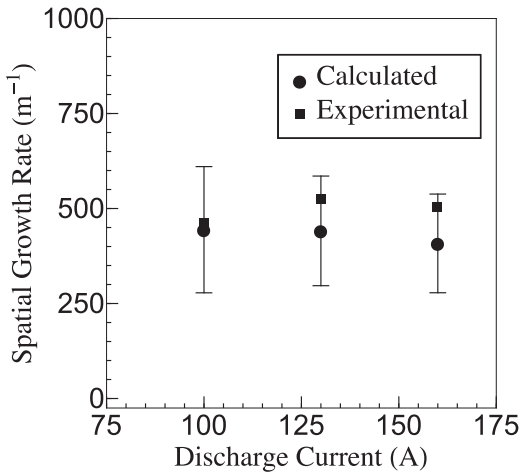

FIG. 12. Measured spatial growth rate, k_i, and average calculated spatial growth rate, $\langle k_{i(L)} \rangle$ for the IAT along cathode centerline.

analytical predictions and experiment is the major finding of this work. Indeed, while it previously has been proposed that a quasilinear formulation may be appropriate to describe the IAT propagation in the hollow cathode plume [9,13], our result provides experimental evidence supporting unambiguously this description for the plume of this high-current device.

V. DISCUSSION

From a practical perspective, the experimental validation of a first-principles theory for IAT growth has direct implications for ongoing efforts to develop predictive and self-consistent models of this region [8,10]. Indeed, two dominant effects in the cathode plume, enhanced electron resistivity and the onset of energetic ions, both have been shown to depend on the total energy density of the IAT [7,15]. To evaluate self-consistently the role of these processes in the plume, there is a need to understand not only how the IAT drives these mechanisms, but more fundamentally, how the IAT itself propagates in this region. We have provided experimental evidence in direct support of one particular hierarchy, a frequency-averaged quasilinear theory, to model the IAT's energy density.

With that said, there are outstanding questions about IAT growth and saturation that are not captured by this formalism. Most notably, although the predicted spatial growth from Fig. 10(b) suggests that the IAT energy should continue to grow at approximately the same exponential rate for the 130 A and 160 A conditions, it actually plateaus in both cases 15–20 mm downstream of the cathode exit (Fig. 11). A possible explanation for this deviation from the quasilinear prediction is that nonlinear mechanisms such as ion trapping or wave-wave interactions lead to the saturation of the growth at high energy densities [28–31]. To explore this hypothesis, we briefly consider here the saturation mechanism, nonlinear ion Landau damping, that leads to the so-called Sagdeev scaling. We choose this particular process as previous numerical modeling works have suggested it may describe the IAT amplitude for some cathode operating conditions [2,11]. The total IAT energy density in the saturated Sagdeev limit has a characteristic algebraic dependence on the background plasma parameters [1]:

$$W_{\text{sat}} = \alpha n_0 T_e \left(\frac{T_e}{T_i} \right) M_e, \tag{13}$$

where $\alpha \sim O[10^{-2}]$ is a constant. We show in Fig. 13 a comparison between the calculated saturated energy density from Eq. (13) (assuming a representative value $\alpha = 3 \times 10^{-2}$) and the measured IAT energy density. In the region where the IAT exhibits quasilinear growth, i.e., from 3–15 mm, W_T is below the Sagdeev saturation limit; however, at the downstream area from 15–20 mm, the IAT energy density becomes comparable to the saturation level. This is precisely the location where the exponential growth gives way to the plateaus for the 130 A and 160 A cases. On the other hand, for the low current case, 100 A, the onset of the saturation does not appear to be as developed in Fig. 13, which is in keeping with the observation that in this region of the plasma, the IAT energy density is still below the Sagdeev limit. For this low current case then, it is possible the wave may continue to grow as it propagates downstream of our experimental region.

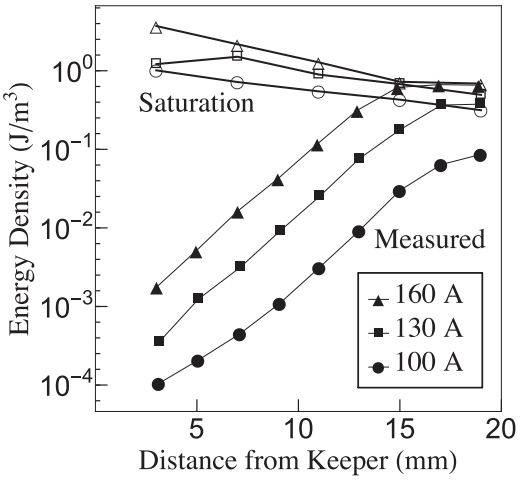

FIG. 13. Plot of the calculated saturation IAT energy density along cathode centerline compared to the measured IAT energy density. The constant used to evaluate the calculated saturation values was $\alpha = 3 \times 10^{-2}$.

The close correspondence between Eq. (13) and the plateaus in IAT growth suggests experimentally that the Sagdeev limit may be a viable mechanism to describe the saturated IAT energy density in the cathode plume. This observation may in fact explain why previous modeling attempts for certain low-current cathodes—the NEXIS and NSTAR discharge devices—were successful even though only simple Sagdeev scaling was assumed to describe the IAT [2,11]. Indeed, in contrast to the results we have shown here, it is possible that the turbulence growth occurred so rapidly in these cathodes that saturation onset immediately downstream of the keeper—thus rendering the Sagdeev scaling appropriate for the majority of the plume.

A comparison of the anticipated growth rates in these other devices with our measured rates provides some evidence to support this claim. The measured densities at centerline for these low current cathodes at the keeper orifice were $n_0 \approx 1$–2×10^{13} cm^{-3} for the NEXIS (Ref. [2], Fig. 3) and NSTAR (Ref. [11], Fig. 14) cathodes. The discharge currents were, respectively, $I_D = 25$ A and $I_D = 13.3$ A, with keeper orifices with radii of $r_k = 2.4$ mm. The electron temperatures ranged from 2.5–3.0 eV, values comparable to those observed in our work. Using the simplification that $M_e \approx I_D/(qn_0A_kv_{te})$, where n_0 is the density on centerline at the keeper exit and A_k is the area of the keeper, we find that the Mach numbers in these two smaller devices may have been larger by a factor of 2–4 compared to the 160 A case we observed here (the configuration with the most evident saturation). This increase stems from the lower plasma density in these other devices coupled with the smaller keeper orifices. Provided the ion Landau damping contributions remained approximately the same as in our case, these higher Mach numbers could have led to wave growth that occurred more rapidly with distance, thereby reaching saturated values at an upstream location in the plume compared to our 160 A result. The validity of the use of a saturated spectrum in these other works therefore may in fact be consistent with the framework we have explored here.

In addition to the issue of saturation, there is another key parameter that we have not been able to derive from the quasilinear formulation, the average growth frequency, ω_0. While we were able to calculate this frequency in this work by measuring the IAT spectrum directly, it is still an open question as to how to describe this property self-consistently. One empirically-driven approximation that is partially supported by the centerline observations in Fig. 8 is to assume ω_0 is constant in the plume. This is the approach currently favored in the numerical cathode model employed in Ref. [8] and has yielded quantitative agreement with experimental measurements. Another possibility to select ω_0 is to consider the relative growth rates in the different modes according to the linear dispersion relation. Indeed, it can be shown that from a full consideration of the dispersion relation of the ion acoustic mode, the wave frequency that leads to the maximum linear growth from the electron Landau damping term follows $\omega_r \sim \omega_{pi}$ where ω_{pi} is the ion plasma frequency. Assuming that this mode with maximum growth dominates the IAT spectrum, then an appropriate substitution may be $\omega_o \propto \omega_{pi}$. This is the approach that Sary *et al.* [9,10] have applied in their numerical models for the IAT. We note, however, that as Fig. 8 shows, $\omega_0 \ll \omega_{pi}$ for our cathode plasma. This suggests that this simplification for the average IAT frequency is not necessarily valid for a real configuration, and indeed, the simulation results by Sary *et al.* in the plume only showed qualitative agreement with experimental measurements of their cathode's plume. The appropriate model for ω_0 is thus still unknown and not readily apparent from our quasilinear description. Ultimately, such a model would require a first-principles, self-consistent description of the IAT spectrum informed by a careful consideration of the several nonlinear mechanisms governing its shape [16].

Leaving aside these open questions about the inability of the quasilinear formulation to predict saturation or the average frequency, there is another notable physical trend in our results that is not addressed by our analytical formulation. This is the observation that although in all three discharge current cases the wave energy grew at approximately the same rate, the three cases exhibited different overall energy magnitudes. Indeed, as Fig. 11 shows, the dependence on discharge current was exponential at each fixed location in the plume. The reason for this trend is not immediately evident from our formulation, but one possible explanation that would fit the observations is that the location where the IAT started to grow moved upstream with discharge current. In this case, although the growth rate remained the same, the total energy of the turbulence that started upstream would be higher than the those with delayed starts. Fitting lines to the exponential growths in Fig. 11 and tracing them back to the starting level exhibited by the 100 A, we can see that the IAT growth for the 130 A case may have started as far upstream as the keeper exit, 0 mm, while the 160 A case may have onset upstream of the keeper exit. The reason why the various cases would have different starting points is not evident from our experimental data, but we do note from previous numerical modeling attempts that IAT is not expected to grow inside the cathode tube where the plasma is highly collisional [2,11]. Analytically, this would be represented in Eq. (10) by a negative value for the growth term on the right hand side. Since we observed IAT in the plume,

there must have been a transition point between the inside of the cathode tube and the plume where the collisional processes in the cathode tube subsided sufficiently to permit wave growth. It is plausible that the disparate plasma conditions associated with the different operating conditions led to a state where the higher current cases could have had positive growth upstream of the lower current cases. Evaluating this possibility and the mechanisms that might contribute to this varying transition point is not addressed here, but a self-consistent, validated numerical model informed by our results here may offer critical insight into this process.

As a final consideration, we note that in focusing on the growth of the IAT, we have treated the plasma parameters that govern its evolution, the plasma density and ion temperature, for example, as independent variables that serve as inputs to the model [Eq. (10)]. This is a valid, self-consistent approach in that although the IAT interacts with and changes the plasma properties, we have measured the plasma conditions at the final steady state, where equilibrium has been reached. In following this approach, it thus has not been necessary to consider directly or model the impact of the IAT on the background plasma parameters. Armed with the knowledge that a quasilinear formulation is appropriate for describing the propagation of the IAT itself, however, we note that a quasilinear or simplified kinetic approach may be appropriate to describe the IAT's interaction with the background plasma processes (cf. Ref. [32]).

VI. CONCLUSION

In this investigation, we have characterized the growth of the energy density of ion acoustic turbulence in the plume of a high-current hollow cathode. We have found that this growth is exponential in the near field region and can be approximated by a conservation equation that stems from a frequency-averaged, quasilinear theory. In this formalism, the IAT is characterized by a total energy density and average frequency, and its growth is the result of a balance between collisionless and collisional processes. We have shown that while inverse electron Landau damping is dominant and ultimately leads to net growth, ion Landau damping also plays a significant role due to the non-negligible ion temperature in the plume. Ion-neutral collisions, on the other hand, appear to have a minimal impact on the observed wave growth. Downstream of the cathode exit, we have found that at higher discharge currents, the growth of the IAT saturates, and the quasilinear formulation no longer applies. However, we have shown that this saturation may be explained by a particular nonlinear process, the Sagdeev limit, that yields predictions commensurate with our experimental results.

In addition to the problem of saturation, we have discussed other aspects of the IAT propagation that were not captured self-consistently with the quasilinear formulation. Most notably, although we were able to measure directly the average frequency of the IAT spectrum in this investigation for the purpose of validating our model for the propagation of the energy density, we do not as yet have a first principles way of calculating this frequency. Moreover, there are still open questions about how the IAT directly leads to some of the key so-called anomalous plasma processes in the plume, enhanced resistivity and ion heating, for example. Although we have refrained explicitly from addressing these mechanisms in this study, we do note that the validation of the quasilinear formulation for the IAT growth suggests that this hierarchy may be appropriate for describing the interactions of the turbulence with the plasma species.

Ultimately, in addition to being of fundamental interest, our experimental validation of the governing relation for IAT propagation lends direct support to on-going efforts to introduce IAT effects self-consistently into cathode models. This finding thus is not only a significant step forward for improving our understanding of the underlying physical processes in the cathode plume but also for developing high-fidelity predictive tools for analyzing these devices.

ACKNOWLEDGMENTS

The research described in this paper was carried out by the Jet Propulsion Laboratory, California Institute of Technology, under a contract with the National Aeronautics and Space Administration. The authors acknowledge the assistance of Amine Elhafsi in preparing the diagnostics and setup and Ray Swindlehurst and Nowell Niblitt for their technical assistance with the facility. The authors also thank Dr. Ioannis Mikellides and Dr. Alejandro Lopez Ortega for their feedback and discussions on this work.

[1] R. Sagdeev and A. Galeev, *Nonlinear Plasma Theory*, Frontiers in Physics (W.A. Benjamin, San Francisco, CA, 1969).

[2] I. G. Mikellides, I. Katz, D. M. Goebel, and K. K. Jameson, J. Appl. Phys. **101**, 063301 (2007).

[3] T. Honzawa and Y. Kawai, Plasma Phys. **14**, 27 (1972).

[4] B. W. Dodson, W. L. McMillan, J. M. Mochel, and R. C. Dynes, Phys. Rev. Lett. **46**, 46 (1981).

[5] H. de Kluiver, N. Perepelkin, and A. Hirose, Phys. Rep. **199**, 281 (1991).

[6] B. Jorns, A. Lopez Ortega, and I. G. Mikellides, Mitigation of energetic ions and keeper erosion in a high-current hollow cathode, in *Proceedings of the 34th International Electric Propulsion Conference (IEPC'15), Hyogo-Kobe, Japan, July 4–10* (Electric Rocket Propulsion Society, Hyogo-Kobe, Japan, 2015).

[7] C. Dodson, D. Perez-Grande, B. Jorns, D. M. Goebel, and R. E. Wirz, Laser-induced fluorescence measurements of energetic Ions in a 100-A LaB6 hollow cathode plume, in *Proceedings of the 52nd AIAA/SAE/ASEE Joint Propulsion Conference (AIAA'16), Salt Lake City, UT. July 25–27* (American Institute of Aeronautics and Astronautics, Salt Lake City, UT, 2016).

[8] A. Lopez Ortega, I. G. Mikellides, and B. Jorns, First-principles modeling of the IAT-driven anomalous resistivity in hollow cathode discharges II: Numerical simulations and comparison with measurements, in *Proceedings of the 52nd AIAA/SAE/ASEE Joint Propulsion Conference (AIAA'16), Salt Lake City, UT. July*

25–27 (American Institute of Aeronautics and Astronautics, Salt Lake City, UT, 2016).

[9] G. Sary, L. Garrigues, and J. P. Boeuf, Plasma Sources Sci. Technol. **26**, 055007 (2017).

[10] G. Sary, L. Garrigues, and J.-P. Boeuf, Plasma Sources Sci. Technol. **26**, 055008 (2017).

[11] I. G. Mikellides, I. Katz, D. M. Goebel, K. Jameson, and J. Polk, J. Propul. Power **24**, 866 (2008).

[12] I. G. Mikellides, D. M. Goebel, B. A. Jorns, J. E. Polk, and P. Guerrero, IEEE Trans. Plasma Sci. **43**, 173 (2015).

[13] B. Jorns, A. Lopez Ortega, and I. G. Mikellides, First-principles modelling of the IAT-driven anomalous resistivity in hollow cathode discharges I: Theory, in *Proceedings of the 52nd AIAA Joint Propulsion Conference (AIAA'16), Salt Lake City, UT. July 25–27* (American Institute of Aeronautics and Astronautics, Salt Lake City, UT, 2016).

[14] T. Stix, *Waves in Plasmas* (AIP, New York, 1992).

[15] B. A. Jorns, I. G. Mikellides, and D. M. Goebel, Phys. Rev. E **90**, 063106 (2014).

[16] V. Bychenkov, V. Silin, and S. Uryupin, Phys. Rep. **164**, 119 (1988).

[17] E. Chu and D. M. Goebel, IEEE Trans. Plasma Sci. **40**, 2133 (2012).

[18] J. M. Beall, Y. C. Kim, and E. J. Powers, J. Appl. Phys. **53**, 3933 (1982).

[19] F. F. Chen, Langmuir probe diagnostics, in *Proceedings of the Mini-Course on Plasma Diagnostics (IEEE-ICOPS'03), Jeju, Korea* (Institute of Electrical and Electronics Engineers, Jeju, Korea, 2003).

[20] B. Jorns, D. M. Goebel, and R. R. Hofer, Plasma perturbations in high-speed probing of hall thruster discharge chambers: Quantification and mitigation, in *Proceedings of the 51st AIAA/SAE/ASEE Joint Propulsion Conference (AIAA'15), July 27–29, Orlando, FL* (American Institute of Aeronautics and Astronautics, Orlando, FL, 2015).

[21] L. Grimaud, A. Pétin, J. Vaudolon, and S. Mazouffre, Rev. Sci. Instrum. **87**, 043506 (2016).

[22] D. M. Goebel, K. K. Jameson, R. M. Watkins, I. Katz, and I. G. Mikellides, J. Appl. Phys. **98**, 113302 (2005).

[23] I. G. Mikellides, I. Katz, D. M. Goebel, and J. E. Polk, J. Appl. Phys. **98**, 113303 (2005).

[24] J. Brophy and C. Garner, Tests of high-current cathodes for ion engines, in *Proceedings of the 24th AIAA Joint Propulsion Conference (AIAA'88), Boston, MA July 11–13* (American Institute of Aeronautics and Astronautics, Boston, MA, 1988).

[25] J. S. Miller, S. H. Pullins, D. J. Levandier, Y. Chiu, and R. A. Dressler, J. Appl. Phys. **91**, 984 (2002).

[26] I. G. Mikellides and I. Katz, J. Propul. Power **24**, 855 (2008).

[27] D. M. Goebel, K. K. Jameson, I. Katz, and I. G. Mikellides, Phys. Plasmas **14**, 103508 (2007).

[28] K. Nishikawa and C. Wu, Phys. Rev. Lett. **23**, 1020 (1969).

[29] A. M. Sleeper, J. Weinstock, and B. Bezzerides, Phys. Fluids **16**, 1508 (1973).

[30] A. Basu, A. S. Sharma, and A. C. Das, Plasma Phys. Controlled Fusion **27**, 433 (1985).

[31] D. Choi and J. Wendell Horton, Phys. Fluids **17**, 2048 (1974).

[32] R. C. Davidson and N. Krall, Nucl. Fusion **17**, 1313 (1977).